

# PCCP

Accepted Manuscript



This is an *Accepted Manuscript*, which has been through the Royal Society of Chemistry peer review process and has been accepted for publication.

*Accepted Manuscripts* are published online shortly after acceptance, before technical editing, formatting and proof reading. Using this free service, authors can make their results available to the community, in citable form, before we publish the edited article. We will replace this *Accepted Manuscript* with the edited and formatted *Advance Article* as soon as it is available.

You can find more information about *Accepted Manuscripts* in the [Information for Authors](#).

Please note that technical editing may introduce minor changes to the text and/or graphics, which may alter content. The journal's standard [Terms & Conditions](#) and the [Ethical guidelines](#) still apply. In no event shall the Royal Society of Chemistry be held responsible for any errors or omissions in this *Accepted Manuscript* or any consequences arising from the use of any information it contains.

# The intermolecular NOE is strongly influenced by diverse dynamical phenomena

Daniel Braun and Othmar Steinhauser

*University of Vienna, Department of Computational Biological Chemistry,  
Währinger Straße 17, 1090 Vienna, Austria*

(Dated: January 15, 2015)

## Abstract

The intermolecular NOE in NMR spectroscopy is analyzed theoretically via computer simulation. Our test case is the homonuclear NOE between hydrogens in the ionic liquid 1-ethyl-3-methylimidazolium trifluoromethanesulfonate. A coarse-grained model of this system is developed and simulated in a 3 microseconds molecular dynamics run, subsequently used for analysis. Our findings are the following: Spin pair specific dynamics has a strong influence on the spectrum. As a consequence, structural information cannot be read off directly. Instead, different contributions to the signals must be disentangled before one can gain information about structure. We show that the extent of signal distortion through dynamics correlates with the spins' distance to their respective molecular centers of mass. Since we deal with pair distributions of spins, the extracted structure does not represent average distances between two spins but the sum of the influence of surrounding spins. In fact, we find that this influence is long-ranged. Our data explicitly shows that the usual  $1/r^6$  dependence is replaced by a distance dependence between  $1/r^3$  and  $1/r$ . However, structural information consists of a spin pair specific short-ranged contribution and a uniform long-ranged contribution. The transition from specific to uniform is sensitive to the behavior of the underlying pair distribution functions.

## I. INTRODUCTION

The nuclear Overhauser effect (NOE) experiment in nuclear magnetic resonance (NMR) spectroscopy is the primary source of structural information, especially in soft matter. Compared to its alternative, diffraction methods, NMR is highly selective and, therefore, also versatile. Furthermore, dynamical structures typical of soft matter can be probed directly in their natural environment without prior preparation.

This has a downside, however: NMR signals always show dynamical features. The NOE does not only record the average dynamical structure but also the rate of change between different structures, i.e., dynamics. More precisely, the vector joining the observed spin pair may change its length and orientation. Both influence the (dipole-dipole) correlation function which makes up the corresponding signal.

We can distinguish between the following two cases: either both spins of a spin pair reside in the same molecule (intramolecular NOE) or they can be found in separate molecules (intermolecular NOE).

In the intramolecular case one usually assumes that the length of the pair vector remains more or less constant, while its orientation is subject to the overall tumbling of the molecule. Thus, one uses the approximation of a uniform tumbling time for all intramolecular pair vectors which can be eliminated from the corresponding signals. This leads to the traditional view that intramolecular NOE signals can be associated with a distance-dependence of  $1/r^6$ .<sup>1,2</sup> Under special conditions, a  $1/r^3$ -averaging formulated by Tropp<sup>3</sup> is used.

For the intermolecular NOE things are quite different. First of all, not only a single pair contributes to the signal but a pair distribution. In other words, the reference spin interacts with corresponding spins on all surrounding molecules. This automatically poses the question of the range of the intermolecular NOE and whether spins at different distances have different effects upon the signals. Of course, spins on different molecules move relative to each other according to molecular translation, thus changing both the length and orientation of the pair vector as a function of time. However, this effect is non-specific among different types of spin pairs and could be eliminated analogously to the overall molecular tumbling in case of the intramolecular NOE. In contrast, in the case of the intermolecular NOE, molecular rotation does not necessarily have a homogeneous effect on all spin pairs and might influence spin pair dynamics in a much more complex way. The investigation of these

characteristic properties of the intermolecular NOE is the topic of this paper.

Excellent reviews of the history of the intermolecular NOE are Refs. 4 and 5. They comprise experimental works concerning electrolyte solutions, mixtures of water with polar solvents, solutions of biomolecules, host-guest complexes etc. and theoretical works concerning model theories. The latter were first formulated by Abragam,<sup>6</sup> who omitted spin specific interaction, reducing the problem to the interaction between molecular centers. In this model, the pair distribution of molecular centers of mass is a step function and the pair dynamics a solution of the diffusion equation of molecular translation. In later works, this model was extended to include off-center effects and rotational diffusion.<sup>7-9</sup> A first attempt to resolve the NOE spatially was made by Halle.<sup>10</sup> A systematic investigation of the range of the NOE was performed recently.<sup>11</sup> An extension of the diffusion model to more complex models of motion can be found in Ref. 12. Examples of experimental studies on the intermolecular NOE in soft matter are Refs. 13–15. While Refs. 13 and 15 present qualitative interpretations of the intermolecular NOE, Ref. 14 investigates the homonuclear  $^1\text{H}$ - $^1\text{H}$  NOE spectrum and assigns distances to signals simply in the spirit of the intramolecular NOE.

Simulation studies of the intermolecular NOE reported so far have pioneer character.<sup>12,16-20</sup> A rather elaborate analysis was recently performed by Shintani *et al.*,<sup>21</sup> who have investigated the dynamics in membranes/micelles. In all of these works, however, because of short simulation times the low-frequency regime of the spectral density function (SDF) was not directly accessible. Depending on the viscosity of the system this would require simulation lengths of hundreds of nanoseconds to several microseconds. Since it was one of the main goals of the present study to calculate the whole range of the SDF directly from simulation data, we developed a coarse-grained (CG) model for our test system, the ionic liquid (IL) 1-ethyl-3-methylimidazolium trifluoromethanesulfonate  $\text{EMIM}^+ \text{OTf}^-$ . The genesis of this model can be found in the first part of the Methods section, while for a more detailed presentation of the force field the reader is referred to the provided Supplementary material. The rest of this paper concentrates on the principles of the intermolecular NOE in soft matter, starting with relevant basics of NMR theory.

## II. THEORY

In an experimental NOE spectrum the signals show the amount of magnetization transfer between spin  $I$  and spin  $S$ . At the macroscopic level, magnetization transfer is described by the second term of the Solomon equation<sup>2</sup>

$$\frac{dM_z^I}{dt} = -(M_z^I - M_{z,0}^I) \rho_{II} - (M_z^S - M_{z,0}^S) \sigma_{IS} \quad (1)$$

where  $M_z$  is the longitudinal magnetization of the system. Without magnetization transfer spin  $I$  would relax according to the longitudinal relaxation rate  $\rho_{II}$ . Taking magnetization transfer into account, the relaxation of spin  $I$  also depends on the relaxation of spin  $S$  via the cross relaxation rate  $\sigma_{IS}$ .

At the molecular level, the relaxation rates depend on the mutual motion of spins in the ensemble. The link between macroscopic and molecular description is provided by the spectral density function  $J(\omega)$ :

$$\rho_{II} = 0.6 J(\omega_I + \omega_S) + 0.3 J(\omega_I) + 0.1 J(\omega_I - \omega_S) \quad (2)$$

for the longitudinal relaxation rate and

$$\sigma_{IS}^{\text{NOESY}} = 0.6 J(\omega_I + \omega_S) - 0.1 J(\omega_I - \omega_S) \quad (3)$$

$$\sigma_{IS}^{\text{ROESY}} = 0.3 J(\omega_I) + 0.2 J(\omega_I - \omega_S) \quad (4)$$

for cross relaxation rates of either the NOESY or the ROESY experiment. In the homonuclear case  $\omega_I = \omega_S$ , and thus  $J(\omega_I - \omega_S) = J(0)$ , the zero-frequency limit of the SDF.

$J(\omega)$  is the Fourier cosine transform of the dipolar correlation function  $G(t)$

$$J(\omega) = K_{IS} \int_0^\infty \cos(\omega t) G(t) dt \quad (5)$$

multiplied by the dipolar coupling constant  $K_{IS}$  which for the NOE between hydrogens is  $\sim 5.7 \cdot 10^{11} \text{ \AA}^6 \text{ s}^{-2}$ .

The mean dipolar correlation function comprising all spin pairs  $IS$  in the system is

$$G(t) = \frac{1}{N_I} \sum_I \sum_S \frac{1}{6} \sum_{\alpha=1}^3 \sum_{\beta=1}^3 \langle T_{IS}^{\alpha\beta}(0) \cdot T_{IS}^{\alpha\beta}(t) \rangle, \quad (6)$$

where the dipole-dipole tensor components  $T_{IS}^{\alpha\beta}$  are

$$T_{IS}^{\alpha\beta}(\vec{r}_{IS}) = \frac{1}{r_{IS}^3} \left\{ \frac{3 r_{IS}^\alpha \cdot r_{IS}^\beta}{r_{IS}^2} - \delta_{\alpha\beta} \right\} \quad (7)$$

and  $\alpha, \beta$  are vector components.

Averaging all tensor components  $T_{IS}^{\alpha\beta}$  in Eq. (6), the angular dependence vanishes at  $t = 0$  and we get

$$\frac{1}{6} \sum_{\alpha=1}^3 \sum_{\beta=1}^3 \langle T_{IS}^{\alpha\beta}(0) \cdot T_{IS}^{\alpha\beta}(0) \rangle = \frac{1}{r_{IS}^6}. \quad (8)$$

Therefore, the amplitude  $A = G(0)$  can be obtained as

$$A = \int_0^{\infty} 4\pi\rho r^2 g_{IS}(r) \frac{1}{r^6} dr \quad (9)$$

where we have replaced the summation over spin pairs in Eq. (6) by an integration over spherical shells weighted by the spin-spin pair correlation function  $g_{IS}(r)$  and the number density  $\rho$ .

Furthermore,  $G(t)$  divided by  $A$  gives the normalized correlation function  $\hat{G}(t)$ . Hence, we can write

$$J(0) = A \cdot \int_0^{\infty} \hat{G}(t) dt = A \cdot \tau \quad (10)$$

where  $\tau$  is defined as the correlation time of  $\hat{G}(t)$ .

It is known from time correlation functions of rather different kinds (velocity<sup>22</sup> and stress-tensor<sup>23</sup> autocorrelation functions) that in the long-time region they obey a hydrodynamic law  $t^{-3/2}$ .<sup>24</sup> This corresponds to a  $-2\sqrt{\omega}$  law in the low-frequency domain,<sup>22,23</sup> as obtained from the rules of the Fourier transform. An analogous behavior

$$J(\omega) = J(0) - b \cdot \sqrt{\omega} \quad (11)$$

was found in the low-frequency regime of NMR NOE spectroscopy, where  $b$  denotes a constant depending on the pair-diffusion coefficient (cf. Ref 25 and references therein).

### III. METHODS

#### A. Genesis of the CG model EMIM<sup>+</sup> OTf<sup>-</sup>

Observables in NMR experiments appear at timescales greater than 100 ns or even 1  $\mu$ s. Especially the homonuclear NOE investigated here depends on very long correlation times (cf. Eqs. (3-6)). Additionally, ionic liquids are highly viscous, and correlations take long

to converge. Hence, a very long trajectory of several  $\mu\text{s}$  is necessary to calculate the desired quantities. In full-atomistic resolution, this would have exceeded reasonable computational effort. Thus, we decided to develop and implement a CG model for the IL 1-ethyl-3-methylimidazolium triflate  $\text{EMIM}^+ \text{OTf}^-$  for this study.

The cation  $\text{EMIM}^+$  is represented as a united-atom model (cf. Fig. 1), where all hydrogens are merged with their respective heavy atom. All parameters for  $\text{EMIM}^+$  are based on previous models but were adapted for our system. Lennard-Jones (LJ) parameters were taken from Ref. 26, where the authors developed a CG model for 1-*n*-butyl-3-methylimidazolium hexafluorophosphate ( $\text{BMIM}^+ \text{PF}_6^-$ ) based on the “optimized potentials for liquid simulations” (OPLS)<sup>27</sup> force field. In our model the butyl chain was shortened to an ethyl chain by eliminating two  $-\text{CH}_2$  united-atom sites. Additionally, the atomic radii  $\sigma$  of the underlying united-atom model were uniformly multiplied by 1.12 to achieve better agreement with experimental density. Partial charges were taken from Ref. 28, and bonded terms were extracted from Ref. 29. The parameter set of our cation model is very similar to the ones’ developed in Ref. 30, where LJ parameters are also based on OPLS and partial charges are obtained by quantum-mechanical calculations as in Ref. 28. The dynamics of these CG models was found to be closer to experiment than dynamics of the slower all-atom (AA) IL models.<sup>31,32</sup> In general, there are many reports of acceleration of dynamics in CG representations of different systems.<sup>33–36</sup>

Most of the existing works on CG models of ILs represent the anion by a single

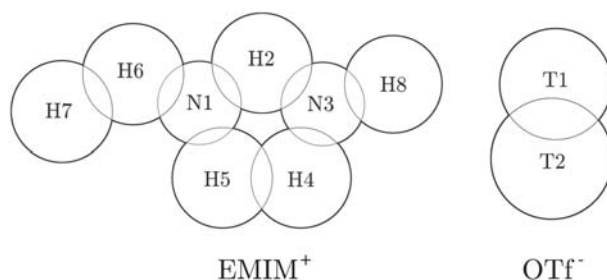


FIG. 1. CG model  $\text{EMIM}^+ \text{OTf}^-$ . The sizes of the spheres match the relative size of the radii  $\sigma$  of the model. In  $\text{EMIM}^+$  H labels united-atom sites of carbons with their respective hydrogen(s), while N labels nitrogens. In  $\text{OTf}^-$  T1 is the coarse-grained  $\text{CF}_3$  site and T2 the  $\text{SO}_3$  site. This CG model maps 27 atoms to 10 sites.

site.<sup>26,30,37-39</sup> However, anisotropy of the ions, both in shape and charge distribution, is essential for molecular ionic liquids. Thus, a single site description of the anion reducing it to a quasi-atomic ion may remove intrinsic qualities of ILs.

Therefore, instead of relying on existing CG models of single-site anions, we developed a two-site model for trifluoromethanesulfonate OTf<sup>-</sup> (cf. Fig. 1). Its charge distribution is based on the AA force field in Ref. 40 as well as the well-depth  $\varepsilon$  of the LJ potentials. The radii  $\sigma$  of the two sites and the molecular geometry (i.e. the distance between the two sites) were optimized to match the packing and orientational structure (cf. Fig. S1 in the Supplementary material) in an iterative procedure, starting out from an intuitive guess.

This bottom-up approach<sup>41</sup> yielded a CG model for EMIM<sup>+</sup> OTf<sup>-</sup> in good agreement with data from AA simulations in terms of structure (packing and mutual orientation) and represents the experimental density and dynamics well. For the sake of completeness, all parameters for this model as well as comparison to AA simulation and experimental data are presented in the Supplementary material.

## B. Simulation

A box of 500 randomly arranged ion pairs of the EMIM<sup>+</sup> OTf<sup>-</sup> model described above was generated using the program PACKMOL.<sup>42</sup> The packed system had to be minimized using the steepest descent method until tolerable energies were reached. This, similar to equilibration and production simulations, was done with version c38b1 of CHARMM.<sup>43</sup>

The equilibration simulation under constant pressure and temperature conditions (Langevin piston method<sup>44</sup>) was part of the model development<sup>44</sup> procedure, because density was a central quantity in determining the force field parameters. The system of 500 ion pairs of the final model (cf. Supplementary material) had an average box side length of 53.8 Å. On the basis of that, a constant volume, constant temperature (NVT) simulation of 100 ns length was performed to equilibrate the system under this thermodynamic regime, followed by a NVT production simulation of 3  $\mu$ s length.

The integration of the equations of motion was done with a time step of 5 fs (via the leapfrog<sup>45</sup> scheme). In a recent work we could show that the larger the time step is, the more it artificially distorts dynamics towards faster dynamics.<sup>46</sup> Since this can have a particularly grave influence on dynamics in CG simulations, we decided to stay on the safe side and not

to exhaust the size of the time step, despite the potential speed-up in production.

Electrostatic interactions were calculated using the particle mesh Ewald method<sup>47</sup> with the Ewald  $\kappa$  parameter set to 0.41 (tin foil boundary conditions) and a  $48 \times 48 \times 48$  grid for the reciprocal space interactions. The cut-off for the real space electrostatic interactions was 12 Å, while Van der Waals interactions were switched off smoothly between 10 and 12 Å.

All bonds were held rigid using the SHAKE algorithm.<sup>48</sup> The average temperature of 300 K was maintained by a Nosé-Hoover thermostat<sup>49,50</sup> with a coupling constant of 1000 kcal mol<sup>-1</sup> ps<sup>2</sup>.

### C. Analysis

All post-simulation analyses were implemented on the basis of MDAnalysis.<sup>51</sup>

As outlined in the theory section, the signals of spin pairs  $IS$  in the ROESY spectrum are obtained from the SDFs  $J(\omega)$  (cf. Eq. (4)), which are the Fourier cosine transform of the dipolar correlation functions  $G(t)$  (cf. Eq. (5)). We calculated  $G(t)$  (cf. Eq. (6)) in the following way: for each spin pair  $IS$  and each element of its respective dipole-dipole tensor  $T_{IS}^{\alpha\beta}(\vec{r}_{IS})$  a separate time correlation function was calculated. Thereby, the trajectory was unfolded to eliminate toroidal jumps, as they usually appear in simulation. In long-term simulation this is necessary to guarantee a continuous time evolution of coordinates and respective pair distances. Consequently, the convolution theorem cannot be applied in this case. In fact, time correlation functions had to be calculated in a direct way, correlating an initial frame with all subsequent frames. Over the 3  $\mu$ s trajectory we defined 20 initial frames separated by 100 ns. For each initial frame all correlation functions were calculated for a total length of 1  $\mu$ s with a spacing of 10 ps. The interaction vectors  $\vec{r}_{IS}$  were calculated directly between the united-atom sites  $H_i$  with  $i_1 \neq i_2$  (cf. Fig. 1) as an approximation to the actual position of the hydrogens. Since this work is of conceptual nature and for reasons of clarity, we separated contributions to the NOE as analyzed from simulation data into its components and extracted only what is of interest here: the intermolecular NOE. In this sense, we do not show intramolecular contributions and ignore the fact that multiple hydrogens at the same chemical shift enhance the signal.

Additional information about the NOE was obtained by resolving the contributions to  $J(\omega)$  spatially. On the one hand, a radial resolution with a bin width of  $\Delta r = 1 \text{ \AA}$  was applied.

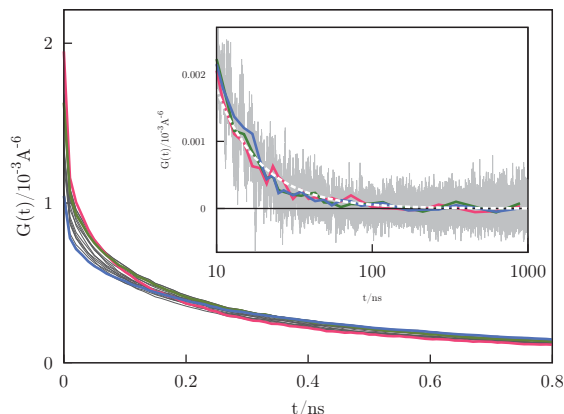


FIG. 2. Dipolar correlation functions  $G(t)$  for the 15 spin pairs under investigation. Colored curves highlight selected spin pairs: H2...H5 in blue; H5...H8 in green; H7...H8 in red. The main plot shows the initial decay in the sub-nanosecond regime. The inset is given on a logarithmic scale and in addition to the three highlighted, averaged and logarithmically thinned spin pairs shows the original data of H5...H8 in light grey as an example. The white dashed line is a fit via a function of the form  $t^{-3/2}$  accurate for all 15  $G(t)$  between 10 and 1000 ns.

On the other hand, we separated the surrounding of a spin into a 1<sup>st</sup> shell, a 2<sup>nd</sup> shell and the bulk. For the definition of molecular shells<sup>52,53</sup> we used the Voronoi algorithm,<sup>54</sup> which is a parameter-free method for a space-filling decomposition of space, attributing an exclusive volume to every site. This second approach allowed us to observe and compare relative contributions of different spins  $S$  inside complete molecular shells around the molecule of spin  $I$ .

#### IV. RESULTS & DISCUSSION

We investigate the intermolecular NOE between hydrogen atoms in the test system EMIM<sup>+</sup> OTf<sup>-</sup>. In this liquid we find hydrogens with 6 different chemical shifts, all of which reside on the cation EMIM<sup>+</sup>. Considering all combinations of hydrogen spins (without self-terms) one gets 15 different spin pairs  $IS$ .

The whole subsequent analysis is based on the dipolar correlation functions  $G(t)$ . For all 15 spin pairs  $IS$  under consideration  $G(t)$  was calculated from the molecular dynamics trajectory of EMIM<sup>+</sup> OTf<sup>-</sup>. corresponding curves are given in Fig. 2. Three selected spin

pairs are highlighted in color: a ring-ring pair H2···H5 in blue, a head-ring pair H5···H8 in green and a head-tail pair H7···H8 in red. To show the spread of behavior of all spin pairs, the remaining ones are shown in grey. This color code applies to every figure in this paper. In the main plot in Fig. 2 one can see a fast decay in the sub-nanosecond region for all spin pairs. Different spin pairs differ in both amplitude and relaxation time to a certain extent. Furthermore, the curves run together in time. For very long times all correlation functions converge and finally fall off together to zero as can be seen in the inset of Fig. 2. It shows the region between 10 and 1000 ns on a logarithmic scale. Here, averaged data of the three selected pairs and, as an example, the non-averaged data of only pair H5···H8 in light grey are given. We want to point out that the whole correlation functions up to 1  $\mu$ s were computed directly from simulation data. The fact that in the time regime of the inset all spin pairs  $IS$  behave practically in the same way implies that characteristics of dynamics at the molecular level are absent, unlike in the beginning of  $G(t)$  (cf. main plot of Fig. 2). In fact, it implies that in the long-time regime the correlation functions depend on pure molecular diffusion, i.e., hydrodynamic behavior. This assumption is supported by a successful fit of all  $G(t)$  from 10 ns to 1  $\mu$ s to the hydrodynamic relation  $t^{-3/2}$  (cf. Sec. II) as shown by a white dashed line in the inset of Fig. 2.

From  $G(t)$  we get the corresponding spectral density functions  $J(\omega)$  (cf. Eq. (5)), which are given in Fig. 3. According to  $G(t)$  extending up to 1  $\mu$ s, the set of  $J(\omega)$  is shown from 1 MHz to 100 GHz on a logarithmic scale. Analogous to the fit  $t^{-3/2}$  to the hydrodynamic region in  $G(t)$  we can describe the region below 100 MHz with the corresponding function in Fourier space  $\sqrt{\omega}$ . The inset shows that in the region below 400 MHz  $J(\omega)$  are indeed almost perfect linear functions of  $\sqrt{\omega}$ . The region below 100 MHz even exhibits strictly parallel lines for all spin pairs  $IS$  and was used for a fit (cf. Eq. (11)), whose parameter  $b$  varies by less than 10% among different spin pairs.

In the region shown in the inset of Fig. 3 it can be seen even more clearly than in Fig. 2 that pair specific dynamics has changed to uniform molecular diffusion.

### A. Spectrum and structure

From  $J(\omega)$  we can now derive the cross-relaxation rates  $\sigma_{IS}$  of the 15 different spin pairs  $IS$ , which make up the signals in NOE spectroscopy. According to Eq. (4) ROESY

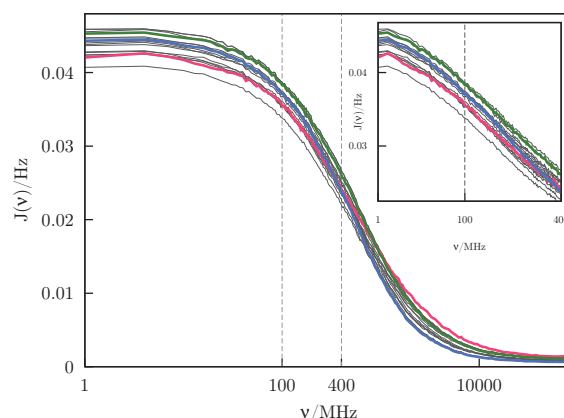


FIG. 3. Spectral density functions  $J(\nu)$  for the 15 spin pairs under investigation calculated from  $G(t)$  given in Fig. 2. Colored curves highlight selected spin pairs: H2...H5 in blue; H5...H8 in green; H7...H8 in red. The main plot shows averaged and logarithmically thinned data over the whole calculated region on a logarithmic scale. Please note how the curves cross each other. The inset plotted on a  $\sqrt{\nu}$  scale and shows that between 1 and 100 MHz different spin pairs are linear and strictly parallel functions of  $\sqrt{\nu}$ , which for the most part holds true in the region between 100 and 400 MHz.

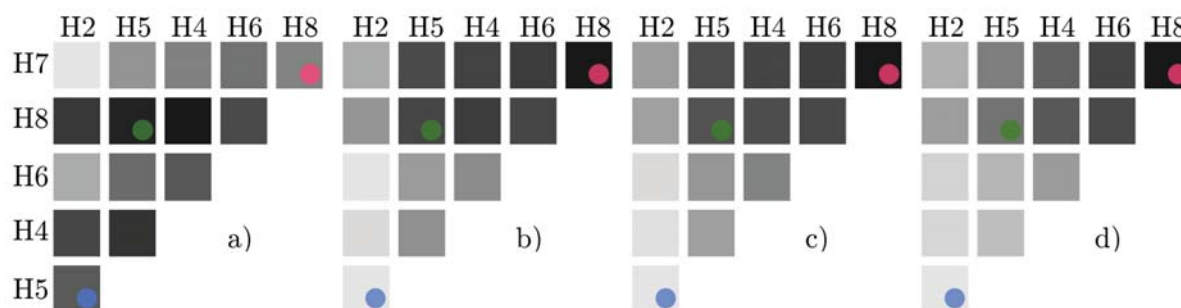


FIG. 4. Schematic intermolecular  $^1\text{H}$ - $^1\text{H}$  ROESY spectra of  $\text{EMIM}^+ \text{OTf}^-$  on a relative scale. Hydrogens are ordered according to their chemical shifts. Intensities rise from white to black. The colored points indicate selected spin pairs as they are highlighted in other figures: H2...H5 in blue; H5...H8 in green; H7...H8 in red. a) Original ROESY spectrum calculated from the SDFs (also representative of  $J(0)$  on the relative scale). b) Reference spectrum showing the structure of the underlying system calculated via Eq. (9) from  $g_{IS}(r)$ . c) Original ROESY spectrum Fig. 4a corrected by dividing each signal by the spin specific relaxation time  $\tau$ . d) Original ROESY spectrum Fig. 4a corrected via the one-parameter model Eq. (12).

cross-relaxation rates are a superposition of the SDF at spectrometer frequency and at the zero frequency limit. For our schematic spectrum the former was taken directly from the calculated SDFs, while the latter was obtained as a parameter  $J(0)$  from the fit (Eq. (11)) from 1-100 MHz as described above.

Fig. 4a shows the collection of the so-obtained  $\sigma_{IS}$  in a schematic ROESY spectrum. Analogous to an experimental 2D spectrum, the signals are ordered according to their chemical shifts and given on a relative scale. The intensity of the signals rises from white to black. In the conventional interpretation the signals are associated with inter-spin distances. Applying this view to the intermolecular ROESY spectrum (Fig. 4a) would imply, e.g., that we find only weak to medium tail-tail (H6...H7) and head-tail (H7...H8) interactions. This seems counter-intuitive because one would expect that proximity of hydrophobic parts is energetically favorable, especially in a highly charged system between ions with like charges.

To test whether intermolecular NOE spectra can be really seen as a direct source of structure information, i.e. the relative strength and ordering of signals are essentially determined by the amplitude  $A$ , we compare Fig. 4a to a hypothetical spectrum Fig. 4b derived from radial distribution functions according to Eq. (9). The discrepancy between Fig. 4a and Fig. 4b is obvious at first sight. Contrary to the ROESY spectrum (Fig. 4a), the underlying structure (Fig. 4b) shows that both head and tail regions are in close proximity to the spins on surrounding molecules. Furthermore, the structure does not exhibit ring-ring contacts (H2...H4, H2...H5, H4...H5), again contradictory to signal strength in the ROESY spectrum. Especially H2 shows only weak signals in the reference spectrum. This is consistent with previously reported structures of ionic liquids where the anion sits around the ring of the cation and especially at position H2.<sup>55</sup>

This comparison leads to the conclusion that in case of the intermolecular NOE the signals are not a direct representation of structure. Instead, spin-spin specific dynamics seems to have a strong influence on the signals. In a recent paper Shintani *et al.* also reported on multiple time scale dynamics associated with the NOE in a micellar system. Please note that in this work the test case is a homogeneous system consisting of small and practically rigid molecules which produces a spectrum characterized by an entanglement of structure and dynamics. Hence, before being able to obtain information about structural properties, dynamics has to be eliminated from the spectrum.

In the SDF the simplest relation between structure and dynamics can be found in

$J(0) = A \cdot \tau$ . For systems of lower viscosity we have extreme narrowing and the signals are proportional to  $J(0)$ . EMIM<sup>+</sup> OTf<sup>-</sup> is a system of higher viscosity, and thus the spectrometer frequency (where the SDF contributes to ROESY signals) falls in the frequency-dependent region of the SDF. However, the inset of Fig. 3 shows almost uniform behavior of all spin pairs not only up to 100 MHz but even 400 MHz (blue and red have the greatest deviation from the mean of all curves). Thus, we can eliminate frequency dependence via the hydrodynamic relation Eq. (11). Combining this relation with Eq. (4), we see that addition of the correction term  $0.3 b\sqrt{\omega_I}$  removes the frequency dependence and leads to signals of strength  $0.5 J(0)$ . Thereby, we use a uniform  $b$  averaged from all fits up to 100 MHz, and we have a constant correction term for all signals. While for further calculations we take the so-obtained absolute  $J(0)$  values, Fig. 4a is still representative of the set of  $J(0)$  on a relative scale.

From the set of  $J(0)$  we can obtain pure structural information  $A$  by dividing  $J(0)$  by  $\tau$ , which is simply the relaxation time of the corresponding normalized correlation function  $\hat{G}(t)$  (cf. Eq. (10)). The result of the new relative intensities can be seen in Fig. 4c. This modified spectrum resembles the structure as it is presented in Fig. 4b almost perfectly. As a result, it is valid to assume that our approach is internally consistent. The main finding is that the intermolecular NOE is indeed strongly influenced by spin pair specific relaxation times  $\tau$  distorting structure information  $A$  in the signals. However, if we have  $J(0)$  and the set of spin pair specific  $\tau$ , this distortion can be removed and the right structure information can be extracted.

In an experimental situation one faces the problem of how to get spin pair specific relaxation times. Broadly speaking,  $\tau$  depends on how the two spins  $I$  and  $S$  move relative to each other. This motion is a superposition of relative translation of respective molecular centers, of overall molecular rotation of both molecules involved, and of intramolecular motion.

Our model system consists of almost rigid molecules and so the intramolecular motion can be neglected. Since molecular translation cannot be spin specific, the effect has to come from molecular rotation only. While the angular velocity of the rotating molecule is the same for all its spins, the orbital speed is not. More precisely, orbital speed is determined by the product of uniform angular velocity times  $\delta$ , the distance of the spin to its respective molecular center of mass. At given angular velocity, the larger  $\delta$  is, the faster the corre-

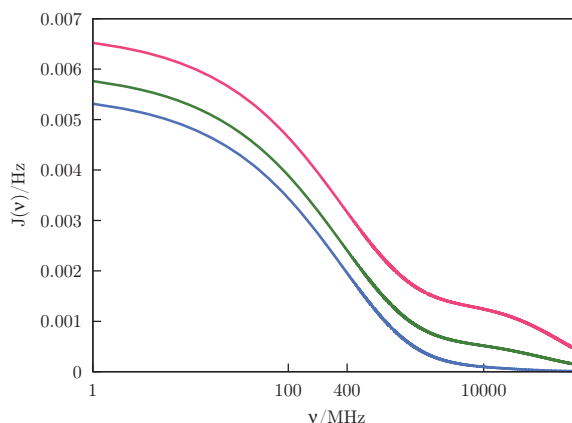


FIG. 5. Spectral density functions calculated via model theory as found in Ref. 10. The three curves differ only in their eccentricity value ( $\delta_I + \delta_S$ ). Through their color they can be compared to corresponding spin pairs in the rest of the paper: blue is calculated with  $(\delta_I + \delta_S)=2$ , green with  $(\delta_I + \delta_S)=4$  and red with  $(\delta_I + \delta_S)=5$ . Please note the difference in frequency-dependent behavior when compared to Fig 3.

sponding site of the spin moves, and thus the decorrelation is suspected to be faster. Indeed, we find that the sum of the distances ( $\delta_I + \delta_S$ ) correlates with spin pair specific  $\tau$ . For the system studied here we even find an astonishingly simple, linear relationship between  $\tau$  of spin pair  $IS$  and  $(\delta_I + \delta_S)$  for  $0 \text{ \AA} \leq (\delta_I + \delta_S) \lesssim 6 \text{ \AA}$ . Correcting the ROESY spectrum with this linear model for  $\tau$

$$J(0)^{corr} = \frac{J(0)}{1 - c \cdot (\delta_I + \delta_S)} \approx A \quad (12)$$

we get the spectrum in Fig. 4d. The fair agreement of the so-corrected spectrum and the structure data (cf. Figs 4d and 4b) demonstrates that a spectrum of the intermolecular NOE distorted by spin pair specific dynamics can be disentangled by a single parameter model, resulting in correct structure information.

With what we have learned, we now want to make reference to previous literature. Most works on the principles of the intermolecular NOE are based on model theories, which also include the off-center effect of spins.<sup>7-9</sup> All of these model theories rest on the same scheme. To test whether they can reproduce the spin pair specific off-center effect on dynamics found in this work, we calculate three SDFs by model theory based on Ref. 7 only differing in  $(\delta_I + \delta_S)$ . In Fig. 5 the curve in blue is  $(\delta_I + \delta_S)=2$  and resembles pair H2...H5; in green we have  $(\delta_I + \delta_S)=4$  resembling pair H4...H5 and in red  $(\delta_I + \delta_S)=5$  for pair H7...H8.

Unlike in the SDFs in this work (Fig. 3), the three curves calculated via model theory do not intersect and their  $J(0)$  become larger with larger  $(\delta_I + \delta_S)$ . Similar curves with and without “excentricity-correction” can be found in Ref. 5. Therefore, one must conclude that model theories in this line are not able to reproduce dynamical effects of the intermolecular NOE in full detail.

Looking at previous experimental works on the intermolecular NOE, we concentrate on Refs. 13 and 14. In imidazolium- IL systems analyzed via the intermolecular NOE they find strong ring-ring contacts. Also in our original ROESY spectrum Fig. 4a we find that ring-ring signals are among the strongest. However, both in the structure and in the spectra corrected for spin pair specific dynamics ring-ring signals are among the weakest. Since all three spins on the ring are in closest proximity to the molecular center of mass, their respective signals are over-emphasized by dynamics relative to other signals stemming from spins which have a greater distance to the molecular center of mass. Our findings provide strong evidence that the qualitative interpretation in Ref 13 and the quantitative analysis in Ref. 14 have to be reconsidered. In fact, Ref. 14 corrected for heterogenous dynamics but only concerning intramolecular flexibility (by a method described in Ref. 56). At last, they did not account for the diversity in dynamics of the intermolecular pair vector. Additionally, a  $1/r^6$  dependence typical for the intramolecular NOE was assumed.

## B. Distance and shell resolution

In the previous section we have analyzed the NOE spectrum with respect to amplitude  $A$  as obtained from spin-spin radial distribution functions  $g_{IS}(r)$ . In this integral  $g_{IS}(r)$  are weighted by  $1/r^4$ . If we look at the underlying Eq. (9), we see that this distance dependence comes about through the dipole-dipole energy  $1/r^6$  times  $r^2$ , which is the population of spins of spherical shells with radius  $r$ . The question arises whether  $1/r^4$  integrated over  $r$  yielding  $1/r^3$  is the final distance dependence in the SDF and, furthermore, whether the spectrum represents the short-range structure or the mean structure over longer distances.

Fig. 6a shows  $g_{IS}(r)$  resolved in molecular shells ( $1^{st}$ ,  $2^{nd}$  and bulk) and Fig. 6b their shell-resolved running integral (cf. Eq. (9)). The  $1^{st}$  shell shows a distinct structure with a pronounced pair specificity which prevails upon integration. In the  $2^{nd}$  shell, however, and even more so in the bulk all pairs have a similar distribution and together with  $1/r^4$  yield

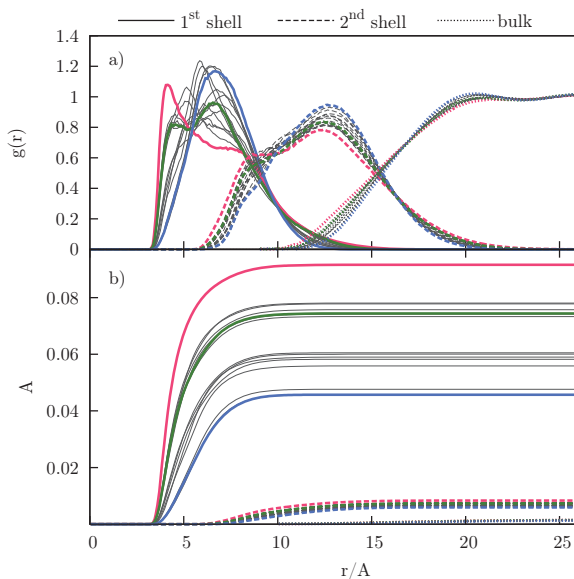


FIG. 6. Shell resolved spin-spin radial distribution functions  $g_{IS}(r)$ . The 1<sup>st</sup> shell is represented by solid lines, the 2<sup>nd</sup> shell by large dashed lines, and the bulk by small dashed lines. Colored curves highlight selected spin pairs: H2...H5 in blue; H5...H8 in green; H7...H8 in red. a) Original  $g_{IS}(r)$  calculated from simulation data. b) Structure information  $A$  obtained from  $g_{IS}(r)$  via Eq. (9).

no specific contribution to the integral.

As already discussed, structure is only one contribution to the SDFs. Applying an analogous procedure of shell decomposition to the SDFs the respective contributions are given in Fig. 7. Again, spin pair specificity is restricted to the 1<sup>st</sup> shell, while the 2<sup>nd</sup> shell and the bulk give almost the same contribution for all spin pairs. Furthermore, shell distance correlates with the frequency-range. The more distant a shell is, the lower are the frequencies it contributes to, as already found by model theory in a previous work.<sup>11</sup> This shell specific frequency-shift further implies that the correlation time  $\tau$  of  $\hat{G}(t)$  also increases with distance.

To get a more rational view on the distance dependence of  $\tau$ , we give radially resolved  $\hat{G}(t)$  in Fig. 8. They are calculated in bins of 1 Å from 3 to 26 Å. The area under  $\hat{G}(t)$ , i.e., the relaxation time  $\tau$  increases monotonically with distance  $r$ . Moreover,  $\tau$  exactly follows a  $r^2$  dependence as can be seen in Fig. 8 by the fit function (ascending curve) to data displayed by circles showing  $\tau$  as a function of  $r$ . This was anticipated by Halle<sup>10</sup> and can be

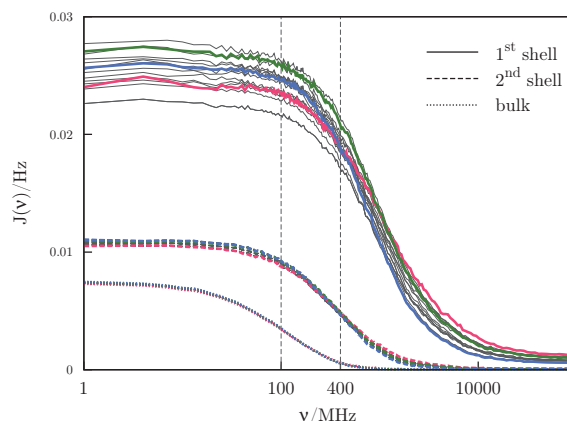


FIG. 7. Shell resolved spectral density functions  $J(\nu)$ . The 1<sup>st</sup> shell is represented by solid lines, the 2<sup>nd</sup> shell by large dashed lines, and the bulk by small dashed lines. Colored curves highlight selected spin pairs: H2...H5 in blue; H5...H8 in green; H7...H8 in red. The data is averaged and thinned logarithmically. Please note how more distant shells yield a uniform contribution to all spin pairs and contribute to lower frequencies of the SDFs.

explained by longer dipole-dipole tensor correlation times caused by slower randomization of the distance vector  $\vec{r}$  migrating on the surface of a sphere of increasing radius  $r$ .

Taking it all together for  $J(0) = A \cdot \tau$ , there are two parabolic amplifiers  $r^2$  when integrating the dipole-dipole energy  $1/r^6$ . On the one hand we have the average number of spins  $4\pi\rho r^2 dr$  and on the other hand the  $r^2$  dependence of the relaxation mechanism, yielding a  $1/r$  dependence for  $J(0)$ . In the extreme narrowing limit the spectrum practically records  $J(0)$ , and this distance dependence holds true. The general case, however, is more complex and the actual range of the NOE depends on both the frequencies at which the SDF is recorded and the dynamics of the system under investigation. For systems with slower dynamics, as in this work, the intermolecular NOE will have a range between  $1/r$  and  $1/r^3$ . One can imagine extrem cases where the NOE is even more short-ranged; this might occur for the heteronuclear NOE of systems with very slow dynamics, simultaneously recorded at very high spectrometer frequencies.

If we look at Fig. 7, we see that in our system all shells but the 1<sup>st</sup> give uniform contributions for all spin pairs. This is because the set of pair distribution functions  $g_{IS}(r)$  converges to a common shape soon after the first shell (cf. Fig. 6). In addition, the weighting of almost  $1/r^2$  in the integral still diminishes the influence of remaining specificity in

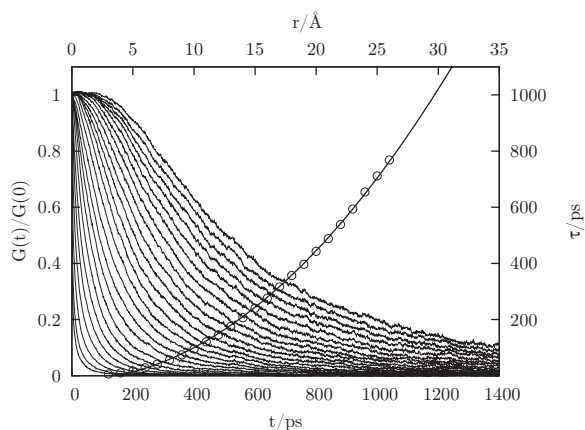


FIG. 8. Distance resolved and normalized dipolar correlation functions  $\hat{G}(t)$  averaged over all spin pairs together with their relaxation time  $\tau$  as a function of distance  $r$ . The decaying curves show  $\hat{G}(t)$  for distance intervals of 1 Å given from 3 to 26 Å. Their  $\tau$ , displayed by circles, get larger with distance  $r$ . A fit (ascending curve) reveals a perfect  $r^2$  dependence.

more distant shells. Hence, they make a non-specific, yet considerable contribution to the SDF (cf. Fig. 7). Therefore, if specificity in  $g_{IS}(r)$  is short-ranged, the intermolecular NOE, despite having a range between  $1/r$  and  $1/r^3$  still has the potential to permit interpretation in structural terms.

## V. CONCLUSION

In the present study we show that in the case of the intermolecular NOE the specific dynamics of different spin pairs has a fundamental influence on the NMR spectrum. A direct qualitative interpretation of the signals in terms of strong/medium/weak fails to provide structural information about the underlying system. However, taking the spin pair specific relaxation times from our analysis, the signal could be corrected for dynamical effects resulting in a correct structural assignment. In an experimental situation the set of dipolar relaxation times cannot be obtained without simplifying assumptions in most cases. Therefore, one needs a rationale for the source of spin pair specific relaxation times. Leaving aside the flexibility of molecules, the dynamics of an intermolecular spin pair depends on molecular translation and rotation. Since the only evident source of spin specific dynamics is their orbital speed upon molecular rotation, we correlated the sum of the off-center

distances of the two spins with the respective specific relaxation time and found a linear relation. Consequently, hope remains that structural information can still be extracted from an experimental intermolecular NOE spectrum.

Another fundamental question concerning the intermolecular NOE is what part of the surroundings of the reference spin contributes to the signal. Our data supports the view that the range of the intermolecular NOE is between  $1/r$  and  $1/r^3$ , depending on both the frequencies at which the SDF is recorded and the dynamics of the system under investigation. However, our data also shows that contributions from spins beyond the first shell, despite being considerably large, are non-specific. This can be attributed to the fast decay of specificity in our spin-spin radial distribution functions. It should be noted that specific signals produced by close pairs will always be augmented by a uniform background of indeterminable size, which changes the ratio between signal strengths. This certainly imposes limitations on the quantitative interpretation of the intermolecular NOE, and deriving distances in the conventional way might not be possible.

Finally, we want to comment on the implications of this work on future computational studies of the intermolecular NOE. We used extensive simulations of  $3 \mu\text{s}$  length of a self-developed coarse-grained model system to calculate the complete time range of the dipolar correlation functions. In the long-time limit all correlation functions showed a uniform, hydrodynamic behavior following a  $t^{-3/2}$  law. Consequently, in the low-frequency regime the SDFs followed the corresponding function in Fourier space with the form  $\sqrt{\omega}$ . This implies that the long-time/low-frequency region can be extrapolated via these functions, thus considerably reducing computational effort.

## VI. ACKNOWLEDGMENTS

This work was supported by project No. P23494 of the FWF Austrian Science Fund as well as the Cluster of Excellence RESOLV (EXC 1069) funded by the Deutsche Forschungsgemeinschaft.

---

<sup>1</sup> K. Wüthrich, *NMR of proteins and nucleic acids* (Wiley, New York, 1986).

<sup>2</sup> D. Neuhaus and M. Williamson, *The Nuclear Overhauser Effect* (VCH, Weinheim, 1989).

- <sup>3</sup> J. Tropp, *J. Chem. Phys.* **72**, 11 (1980).
- <sup>4</sup> H. Mo and T. C. Pochapsky, *Progress in Nuclear Magnetic Resonance Spectroscopy* **30**, 1 (1997).
- <sup>5</sup> A. Bagno, F. Rastrelli, and G. Saielli, *Progress in Nuclear Magnetic Resonance Spectroscopy* **47**, 41 (2005).
- <sup>6</sup> A. Abragam, Clarendon, Oxford (1961).
- <sup>7</sup> Y. Ayant, E. Belorizky, J. Aluzon, and J. Gallice, *Journal de Physique* **36**, 991 (1975).
- <sup>8</sup> Y. Ayant, E. Belorizky, P. Fries, and J. Rosset, *Journal de Physique* **38**, 325 (1977).
- <sup>9</sup> P. Fries and E. Belorizky, *Journal de Physique* **39**, 1263 (1978).
- <sup>10</sup> B. Halle, *The Journal of Chemical Physics* **119**, 12372 (2003).
- <sup>11</sup> S. Gabl, O. Steinhauser, and H. Weingärtner, *Angewandte Chemie* **125**, 9412 (2013).
- <sup>12</sup> S. Gabl, C. Schröder, D. Braun, H. Weingärtner, and O. Steinhauser, *The Journal of chemical physics* **140**, 184503 (2014).
- <sup>13</sup> R. A. Mantz, P. C. Trulove, R. T. Carlin, and R. A. Osteryoung, *Inorganic Chemistry* **34**, 3846 (1995).
- <sup>14</sup> A. Mele, G. Romanò, M. Giannone, E. Ragg, G. Fronza, G. Raos, and V. Marcon, *Angewandte Chemie International Edition* **45**, 1123 (2006).
- <sup>15</sup> Y. Lingscheid, S. Arenz, and R. Giernoth, *ChemPhysChem* **13**, 261 (2012).
- <sup>16</sup> P.-O. Westlund and R. Lynden-Bell, *Journal of Magnetic Resonance (1969)* **72**, 522 (1987).
- <sup>17</sup> L. Laaksonen and J. B. Rosenholm, *Chemical physics letters* **216**, 429 (1993).
- <sup>18</sup> J.-P. Grivet, *The Journal of chemical physics* **123**, 034503 (2005).
- <sup>19</sup> J. Gerig, *Molecular Simulation* **38**, 1085 (2012).
- <sup>20</sup> J. Gerig, *The Journal of Physical Chemistry B* **116**, 1965 (2012).
- <sup>21</sup> M. Shintani, K. Yoshida, S. Sakuraba, M. Nakahara, and N. Matubayasi, *J. Phys. Chem. B* **115**, 9106 (2011).
- <sup>22</sup> D. Levesque and W. T. Ashurst, *Phys. Rev. Lett.* **33**, 277 (1974).
- <sup>23</sup> D. J. Evans, *Journal of Statistical Physics* **22**, 81 (1980).
- <sup>24</sup> J. P. Hansen and I. R. McDonald, *Theory of Simple Liquids*, 2nd ed. (Elsevier, 1986) p. 296.
- <sup>25</sup> D. Kruk, R. Meier, and E. A. Rössler, *Phys. Rev. E* **85**, 020201 (2012).
- <sup>26</sup> J. K. Shah, J. F. Brennecke, and E. J. Maginn, *Green Chem.* **4**, 112 (2002).
- <sup>27</sup> W. L. Jorgensen, J. D. Madura, and C. J. Swenson, *J. Am. Chem. Soc.* **106**, 813 (1984).
- <sup>28</sup> C. G. Hanke, S. L. Price, and R. M. Lynden-Bell, *Mol. Phys.* **99**, 801 (2001).

- <sup>29</sup> J. N. Canongia Lopes, J. Deschamps, and A. A. H. Pádua, *J. Phys. Chem. B* **108**, 2038 (2004).
- <sup>30</sup> S. M. Urahata and M. C. C. Ribeiro, *J. Chem. Phys.* **120**, 1855 (2004).
- <sup>31</sup> J. Pićálek and J. Kolafa, *Mol. Sim.* **35**, 685 (2008).
- <sup>32</sup> S. M. Urahata and M. C. C. Ribeiro, *J. Chem. Phys.* **122**, 024511 (2005).
- <sup>33</sup> C. F. Lopez, P. B. Moore, J. C. Shelley, M. Y. Shelley, and M. L. Klein, *Comput. Phys. Commun.* **147**, 1 (2002).
- <sup>34</sup> C. F. Lopez, S. O. Nielsen, P. B. Moore, J. C. Shelley, and M. L. Klein, *J. Phys. Condens. Matter* **14**, 9431 (2002).
- <sup>35</sup> S. O. Nielsen, C. F. Lopez, G. Srinivas, and M. L. Klein, *J. Phys. Condens. Matter* **16**, R481 (2004).
- <sup>36</sup> Y. Wang, S. Izvekov, T. Yan, and G. A. Voth, *J. Phys. Chem. B* **110**, 3564 (2006).
- <sup>37</sup> D. Roy, N. Patel, S. Conte, and M. Maroncelli, *J. Phys. Chem. B* **114**, 8410 (2010).
- <sup>38</sup> D. Roy and M. Maroncelli, *J. Phys. Chem. B* **114**, 12629 (2010).
- <sup>39</sup> C. Merlet, M. Salanne, and B. Rotenberg, *J. Phys. Chem. C* **116**, 7687 (2012).
- <sup>40</sup> J. N. Canongia Lopes and A. A. H. Pádua, *J. Phys. Chem. B* **108**, 16893 (2004).
- <sup>41</sup> W. G. Noid, *J. Chem. Phys.* **139**, 090901 (2013).
- <sup>42</sup> L. Martínez, R. Andrade, G. Birgin, and J. M. Martínez, *J. Comput. Chem.* **30**, 2157 (2009).
- <sup>43</sup> B. R. Brooks, C. L. Brooks III, A. D. MacKerell Jr., L. Nilsson, R. J. Petrella, B. Roux, Y. Won, G. Archontis, C. Bartels, S. Boresch, A. Caffisch, L. Caves, Q. Cui, A. R. Dinner, M. Feig, S. Fischer, J. Gao, M. Hodoseck, W. Im, K. Kuczera, T. Lazaridis, J. Ma, V. Ovchinnikov, E. Paci, R. W. Pastor, C. B. Post, J. Z. Pu, M. Schaefer, B. Tidor, R. M. Venable, H. L. Woodcock, X. Wu, W. Yang, D. M. York, and M. Karplus, *J. Comput. Chem.* **30**, 1545 (2009).
- <sup>44</sup> S. E. Feller, Y. Zhang, R. W. Pastor, and B. R. Brooks, *J. Chem. Phys.* **103**, 4613 (1995).
- <sup>45</sup> R. W. Hockney, *Meth. Comput. Phys.* **9**, 136 (1970).
- <sup>46</sup> D. Braun, S. Boresch, and O. Steinhauser, *J. Chem. Phys.* **140**, 064107 (2014).
- <sup>47</sup> U. Essmann, L. Perera, M. L. Berkowitz, T. Darden, H. Lee, and L. G. Pedersen, *J. Chem. Phys.* **102**, 8577 (1995).
- <sup>48</sup> J.-P. Ryckaert, G. Ciccotti, and H. J. C. Berendsen, *J. Comput. Phys.* **23**, 327 (1977).
- <sup>49</sup> S. Nosé, *J. Chem. Phys.* **81**, 511 (1984).
- <sup>50</sup> W. G. Hoover, *Phys. Rev.* **A31**, 1695 (1985).

- <sup>51</sup> N. Michaud-Agrawal, E. J. Denning, T. B. Woolf, and O. Beckstein, *J. Comput. Chem.* **32**, 2319 (2011).
- <sup>52</sup> C. Schröder, G. Neumayr, and O. Steinhauser, *J. Chem. Phys.* **130**, 194503 (2009).
- <sup>53</sup> G. Neumayr, T. Rudas, and O. Steinhauser, *The Journal of chemical physics* **133**, 084108 (2010).
- <sup>54</sup> C. Rycroft, *Chaos* **19**, 041111 (2009).
- <sup>55</sup> C. Schröder, T. Rudas, and O. Steinhauser, *J. Chem. Phys.* **125**, 244506 (2006).
- <sup>56</sup> J. H. Antony, A. Dölle, D. Mertens, P. Wasserscheid, W. R. Carper, and P. G. Wahlbeck, *J. Phys. Chem. A* **109**, 6676 (2005).